Mon. Not. R. Astron. Soc. **000**, 000–000 (0000) Printed 15 December 2014 (MN LATEX style file v2.2)

Light versus Dark in Strong Lensing Galaxies: Dark matter halos are rounder than their stars

Claudio Bruderer[1⋆], J. I. Read[1,2], P. Saha[3], J. Coles[4]
[1] *Institute for Astronomy, Department of Physics, ETH Zürich, Wolfgang-Pauli-Strasse 27, CH-8093 Zürich, Switzerland*
[2] *Department of Physics, University of Surrey, Guildford, GU2 7XH, UK*
[3] *Institute for Theoretical Physics, University of Zürich, Winterthurerstrasse 190, 8057 Zürich, Switzerland*
[4] *Exascale Research Computing Lab, Campus Teratec, 2 Rue de la Piquetterie, 91680 Bruyeres-le-Chatel, France*

15 December 2014

ABSTRACT

We measure the shape and alignment of stars and dark matter in 11 strong lensing galaxies and find that in all cases the dark matter halos are rounder than the light distribution over the range $R_e < R < 5R_e$. Averaging over larger radii, the lenses become increasingly elliptical both in their dark matter and stellar components, as defined using the ratio s of the largest to smallest eigenvalues of the 2D moment of inertia tensor of the projected lensing mass. While dark matter halos are never more elliptical than $s_{dm} = 1.15$, their stars can extend to $s_* > 1.4$ Three systems, in particular, have very high stellar ellipticity ($s_* > 1.6$) and correspondingly high alignment between light and dark. One of these – B1608 – is a known merging pair; we suggest that the other two (B0712 and B2016) may also be recent post-merger systems. Galaxies with high dark matter ellipticity and weak external shear show very strong alignment between light and dark; those with strong shear ($\gamma \gtrsim 0.1$) can be very highly misaligned. This is reassuring since isolated misaligned galaxies are expected to be unstable.

Our results provide a new constraint on galaxy formation models that must explain the origin of very round dark matter halos and highly misaligned systems. Such misalignments also present a new challenge for alternative gravity theories in which the light and dark must necessarily be highly correlated.

Key words: Gravitational lensing: strong — galaxies: structure

1 INTRODUCTION

The ellipticity and shape of stars relative to their host dark matter halo encodes information both about our cosmological model (ΛCDM) and galaxy formation (e.g. Dubinski 1994; Ibata et al. 2001; Kazantzidis et al. 2004; Macciò et al. 2007; Debattista et al. 2008; Lux et al. 2012; Read 2014). 'Dark-matter-only' (DMO) simulations in ΛCDM predict dark matter halos that are triaxial (Dubinski & Carlberg 1991; Warren et al. 1992; Navarro et al. 1996; Jing & Suto 2002), with mean 'shape parameter' $\langle q \rangle = (b + c)/2a \sim 0.8$ (where $a > b > c$ are the long, intermediate and short axes of the figure; Macciò et al. 2007). This corresponds to a typically *prolate* halo. However, including 'baryons' (stars and gas) in the models produces halos that are significantly rounder and – at least for disc galaxies – well-aligned with the light distribution (Katz & Gunn 1991; Dubinski 1994; Debattista et al. 2008). Halo shapes and alignments also constrain alternative gravity models (Mortlock & Turner 2001; Helmi 2004; Read & Moore 2005; Ferreras et al. 2012; Debattista et al. 2013). If the visible light is the only source of gravity in a galaxy, then we expect the light and mass distribution to be highly correlated; if dark matter is present, however, such correlations can, at least in principle, be broken.

Strong lensing provides a unique probe of the alignment and shape of the total mass distribution in galaxies (e.g. Blandford & Narayan 1986; Schneider et al. 1992; Keeton et al. 1998; Kochanek et al. 2000; Koopmans et al. 2006; Auger et al. 2007; Ferreras et al. 2008; Auger et al. 2010; Leier et al. 2012). For 'red and dead' ellipticals that are largely devoid of gas, their baryonic content can be mapped through stellar population synthesis modelling of their light distribution (e.g. Ferreras et al. 2005; Treu et al. 2006; Ferreras et al. 2008). This opens up the possibility of directly comparing the light and mass in strong lensing systems (Keeton et al. 1998; Ferreras et al. 2008; Treu et al. 2009; Sluse et al. 2012). Previous work in the literature has found

⋆ E-mail: claudio.bruderer@phys.ethz.ch

that the light and mass are well-aligned (though a mis-match of up to 10° is not uncommon; e.g. Sluse et al. 2012). However, results on the ellipticity of light and mass agree less well, with Sluse et al. (2012) finding a strong correlation and Keeton et al. (1998) and Ferreras et al. (2008) finding none. It is difficult, however, to compare the results between these different studies because they use different lens modelling techniques; different definitions of ellipticity; and different radii over which the shapes and alignments are probed. Furthermore, none to date have applied their methodology to mock data to determine the robustness of the results.

Weak lensing can also be used to probe the shape and alignment between light and dark, but only for 'stacked' galaxies (Brainerd & Wright 2000; Natarajan & Refregier 2000). Hoekstra et al. (2004) applied this idea to data from the Red-Sequence Cluster Survey (RCS) to measure the first weak lensing signal of halo flattening. They found that dark matter halos appear to be rounder then their light distributions, with some weak evidence for alignment. Both measurements are challenging, however, and more recent data appear to be at odds with this early work, favouring dark matter halos that are more elliptical than their stars (Mandelbaum et al. 2006; Parker et al. 2007; van Uitert et al. 2012).

Recently, we introduced a new non-parametric lens tool, Glass (Coles et al. 2014). Applying this to a large suite of mock data, we showed that mass and light can only reliably be disentangled in strong lensing systems if: i) there are at least four images; and ii) time delay data are available and/or the stellar mass dominates the potential over the region of the images. **CB. i) is the case for all the lenses, ii) however only for a minority of the sample. This sentence creates therefore some tension that is not addressed however (I don't know whether we should rephrase it or add another sentence).** In this paper, we collate data of the above quality, compiling a sample of 11 strong lens galaxies. We apply Glass to these lenses to non-parametrically measure the shape and alignment of the stars and *dark matter* in these lensing galaxies, for the first time. This differs from previous works that have all compared the light distribution with the total mass, rather than the dark matter. Since the stars often dominate the central potential, the total mass naturally correlates with the light, potentially masking theoretically interesting results about the dark matter distribution. Our comparison between light and dark is made possible by the fact that Glass uses the light distribution as a prior on the mass map, ensuring that the dark matter mass is always positive.

This paper is organised as follows. In §2, we briefly review the Glass code. In §3, we present our data compilation with references. In §4, we present our results. Finally, in §5 we discuss the implications of these results and we present our main conclusions.

2 Glass: A NON-PARAMETRIC LENS TOOL

Glass is a new 'non-parametric' gravitational lens modelling framework (Coles et al. 2014) that is capable of generating a distribution of mass models given a set of basic assumptions, or priors. In this context, non-parametric means that many more parameters than data constraints are used such that system of equations describing the lensing mass distribution is under-constrained. Glass shares some aspects with an earlier code PixeLens (Saha & Williams 2004; Coles 2008), but has a completely different code base. Its key improvements upon PixeLens which are relevant for this paper include:

(i) A new uniform sampling algorithm for high dimensional spaces (Lubini & Coles 2012). This allows for large ensembles of $> 10,000$ models to be efficiently generated.
(ii) With so many models in the final ensemble, we can afford to apply non-linear constraints (for example stellar kinematic data; or the removal of models with spurious extra images) to accept/reject models in a post-processing step.
(iii) The central region of the mass map can have a higher resolution to more efficiently capture steep models.
(iv) Stellar density can be used as an additional lower-bound constraint on the models.

In this paper, the default priors used to model each lens are listed below. Table 2 identifies lenses for which we have modified these defaults. For each lens we assume:

(i) Observational priors (redshifts, image positions relative to lens position).
(ii) Image parity is enforced.
(iii) A reconstructed stellar mass map.
(iv) The local density gradient is always pointing within 50° to the center and the slope is at most 0 everywhere. In other words, the density profile peaks in the center.
(v) The fixed cosmology $\Omega_m = 0.28$, $\Omega_\Lambda = 0.72$, $\Omega_k = 0$, $H_0^{-1} = 13.7$ Gyr.
(vi) A flat prior on the magnitude of the external shear $|\gamma|$ on $[0, 1)$.

In cases where more information is available, the following priors are also used:

(vii) A flat prior on measured time delays within the $\pm 1\sigma$-interval.
close to the Einstein radius.
(viii) Point symmetry $\kappa(x, y) = \kappa(-x, -y)$ where the surface mass profile can be assumed to be symmetric (3+1 quad configurations and the double *Q0957*).

2.1 Measuring the shape and alignment of a lens

JR. WE NEED TO DEFINE OUR SHAPE PARAMETER AND ANALYSIS METHOD HERE. JR. WE NEED TO ALSO DEFINE R_e HERE AND EXPLAIN THAT WE AVERAGE SHAPE OVER 1-5R_e CB. I will write this.

3 DATA

CB. Do we need to add a bit describing the stellar population synthesis modelling? Can maybe Prasenjit write this?

Q0047-2808 (hereafter *Q0047* or *0047*) is a luminous early-type galaxy (Warren et al. 1996). Wong et al. (2011) find a group of 9 members all of which are spectroscopically confirmed.

MG0414+0534 (hereafter *0414*) is a passively evolving early-type galaxy (Tonry & Kochanek 1999). Schechter & Moore (1993) find a very close luminous satellite galaxy north-west of the lens. (Curran et al. 2011) however conclude that it is more likely a foreground object.

B0712+472 (hereafter *0712*) is an early-type galaxy (Fassnacht & Cohen 1998).

RXJ0911+0551 (hereafter *0911*) is an almost circular early-type galaxy (Sluse et al. 2012). It has measured time delays (Hjorth et al. 2002). It lies on the outskirts of a cluster (Morgan et al. 2001). X-ray emission can be detected and an analysis of which yields a temperature of 2.3 keV. There is also a satellite galaxy to the north-west direction (Kneib et al. 2000).

Q0957+561 (hereafter *0957*) is a cD galaxy lying close to the center of a cluster with a high sprial galaxy-fraction (e.g. Garrett et al. (1992); Angonin-Willaime et al. (1994); Chartas et al. (1998)). Due to the large image separation, large physical scales are probed. As listed in Table 3 of Keeton et al. (2000), the position angles to the center of the cluster of earlier lens reconstructions range between 51.8 deg and 67.8 deg measured north-through-east. These results are consistent with the center of the X-ray emission from the cluster (Chartas et al. 1998). The lens has a measured time delay, e.g. (Shalyapin et al. 2012). They however also find a three-day lag between the g- and r-bands, and the estimates do not agree at the 2σ-level. They argue that this effect can be accounted for by the presence of a substructure and chromatic dispersion. We find that the results do not change significantly for either estimate and choose therefore the g-band measurement.

PG1115+080 (hereafter *1115*) is an early-type galaxy (Yoo et al. 2005). It has measured time delays. We use recent estimates of the time delays by Tsvetkova et al. (2010) which differ from previously found values by e.g. Barkana (1997). Momcheva et al. (2006) and Wong et al. (2011) analyzed the environment of the lens thouroughly. It is part of a small group of 13 members. Grant et al. (2004) detect also X-ray emission from the corresponding group, which yields a temperature of 0.8 keV.

B1422+231 (hereafter *1422*) is an early-type galaxy (Impey et al. 1996). Although there are measured time delays by Patnaik & Narasimha (2001), they seem to deviate significantly from theoretical expectations in Raychaudhury et al. (2003). We choose therefore not to include them in the analysis. Momcheva et al. (2006) find a group environment with 16 spectroscopically confirmed member galaxies. Using newer data, Wong et al. (2011) find an additional member. Grant et al. (2004) also detect X-ray emission from the corresponding group at a temperature of 1.0 keV.

B1608+656 (hereafter *1608* or *1608*) consists of two merging galaxies. The main galaxy is an early-type galaxy which is disrupted by a smaller, probably late-type galaxy (Surpi & Blandford 2003). The system has measured time delays (Fassnacht et al. 2002). The environment and the mass distribution along the line of sight have been analyzed by Fassnacht et al. (2006). They find a group with 8 (9 if merging galaxies are counted individually). No significant X-ray emission was detected from the surrounding group (Dai & Kochanek 2005). The data seems to indicate four other groups along the line of sight.

MG2016+112 (hereafter *2016*) is a giant elliptical galaxy (Lawrence et al. 1984; Schneider et al. 1986). It is the farthest lens we consider in this sample. It lies in a cluster which consists of 69 probable galaxies (Toft et al. 2003). The clusters shows a high density of galaxies close to the lens in a south-east direction.

B2045+265 (hereafter *2045*) is probably an elliptical galaxy (McKean et al. 2007). Fassnacht et al. (1999) initially classified the galaxy as a late-type Sa galaxy, the velocity dispersion however seems too high. As the source redshift is rather low, a large lens mass is required. McKean et al. (2007) therefore conclude that it is more likely an elliptical galaxy. To the west of the lens, Fassnacht et al. (1999) find a group at a similar redshift as the lens. McKean et al. (2007) also find evidence for a dwarf satellite galaxy. As the measurements are inconclusive, we choose to not include this satellite.

Q2237+030 (hereafter *2237*) is a barred spiral (Yee 1988). With only a redshift of $z = 0.04$, it is the closest lens of the sample. Due to the low redshift, the probed physical scales are small. No further inquiries into the environment were made.

Further information about the sample can be found in Leier (2011), Leier et al. (2011), and Sluse et al. (2012).

4 RESULTS

JR. CLAUDIO OR JUSTIN TO WRITE RESULTS SECTION? Content:

- Describe special features in reconstructed lenses
- Show the wedges money plot
- Discuss the results, especially:
- 1. Dark matter halos seem quite round, stars not necessarily
- 2. Both DM and stars more elliptical with increasing radius
- 3. DM halos with weak shear are aligned (apart from spherical systems that don't count); strong shear systems can be highly misaligned.
- 4. No sensitivity to shear prior. Only one lens B2045 requires a shear prior to avoid spurious extra images; doesn't affect the shape measure though.
- 5. Merger systems stand out.

5 CONCLUSION

We have measured the shape and alignment of stars and dark matter in 11 strong lensing galaxies using a new non-parametric lens tool, Glass. We focussed on lenses that have either time delay data or stellar mass maps that contribute significantly to the central potential, since these have data quality good enough to determine the projected shape of their dark matter halos (Coles et al. 2014). We measured the shape and alignment using the eigenvalues λ and vectors of the 2D moment of inertia tensor of the stars and dark matter, defining a *shape parameter* $s = \lambda_{\max}/\lambda_{\min}$ (§2.1). We averaged s over the range 1-5R_e, where R_e is the effective radius of the light profile.

Our key results are as follows:

Lens	z_L	z_S	$\Delta\theta$ [kpc]	R_L/R_e	Environment
0047	0.485	3.60	12.82	1.45 ± 0.04	G(9)
0414	0.960	2.64	16.01	1.85 ± 0.05	...
0712	0.410	1.34	6.82	1.15 ± 0.03	...
0911	0.769	2.8	23.16	3.09 ± 0.05	C
0957	0.356	1.41	29.98	3.51 ± 0.04	C
1115	0.310	1.72	10.76	2.94 ± 0.06	G(13)
1422	0.337	3.62	6.02	4.49 ± 0.06	G(17)
1608	0.630	1.39	13.92	1.82 ± 0.01	G(8)
2016	1.010	3.3	26.22	6.12 ± 0.14	C(69)
2045	0.870	1.28	14.46	1.48 ± 0.03	...
2237	0.039	1.7	1.40	0.89 ± 0.01	...

Table 1. The most relevant lens properties for this work are listed (for an expanded version of this table see Leier et al. 2011). References can be found in §3.

Lens	A ["]	B ["]	C ["]	D ["]	Time delays [days]	Additional priors
0047	1.270	-0.630	0.520	-0.730	...	
	0.105	-0.995	-1.045	0.705		
0414	-0.472	-1.061	-1.1947	0.885	...	
	1.277	-0.661	-0.255	-0.361		
0712	-0.013	0.795	0.747	-0.391	...	
	-0.804	-0.156	-0.292	0.307		
0712	-0.013	0.795	0.747	-0.391	...	
	-0.804	-0.156	-0.292	0.307		
0957[a]	1.408	0.182	2.860	-1.540	$\Delta t_{BA} = 416.5^{+1}_{-1}$	Symm
	5.034	-1.018	3.470	-0.050		
1115	0.355	-0.909	-1.093	0.717	$\Delta t_{BA} = 12.0^{+2}_{-2}$ $\Delta t_{DC} = 4.4^{+3.2}_{-2.4}$	
	1.322	-0.714	-0.260	-0.627		
1422	1.079	0.357	0.742	-0.205	...	Symm
	-0.095	0.973	0.656	-0.147		
1608	-1.300	-0.560	-1.310	0.570	$\Delta t_{BA} = 31.5^{+2}_{-1}$ $\Delta t_{CA} = 36.0^{+1.5}_{-1.5}$ $\Delta t_{DA} = 77.0^{+2}_{-1}$	
	-0.800	1.160	0.700	-0.080		
2016	-1.735	0.335	0.437	1.268	...	
	1.778	-1.450	-1.435	0.276		
2045	1.121	1.409	1.255	-0.507	...	$\gamma(0.1)$, Symm
	0.824	0.035	0.576	-0.183		
2237	0.598	-0.075	0.791	-0.710	...	
	0.758	-0.939	-0.411	0.271		

Table 2. The lens properties relevant for modelling the lenses are listed (positions and time delay information). The images are ordered in terms of arrival time (image A has the shortest arrival time, image D the longest).
[a] The source lensed by 0957 has different component. Images A and B are a double associated with the main galaxy component, images C and D are associated with lensed substructure.

• We found that in all cases the dark matter halos are rounder than the light distribution over the range $R_e < R < 5R_e$. As we average over larger radii, the lenses become increasingly elliptical both in their dark matter and stars, but dark matter halos are never more elliptical than $s_{dm} = 1.15$, while their stars can extend to $s_* > 1.4$.

• Three systems have very high stellar ellipticity ($s_* > 1.6$) and correspondingly high alignment between light and dark. One of these – B1608 – is a known merging pair; we suggest that the other two (B0712 and B2016) may also be recent post-merger systems.

• Galaxies with high dark matter ellipticity and weak external shear show strong alignment between light and dark; those with strong shear ($\gamma \gtrsim 0.1$) can be highly misaligned. This is reassuring since isolated misaligned galaxies are expected to be unstable.

Our results provide a new constraint on galaxy formation models that must explain the origin of very round dark matter halos (not expected in pure dark matter only simulations), and highly misaligned systems. Such misalignments also present a new challenge for alternative gravity theories in which the light and dark must necessarily be highly correlated.

6 ACKNOWLEDGEMENTS

We would like to thank Dominik Leier for useful discussions. JIR would like to acknowledge support from SNF grant PP00P2_128540/1.

REFERENCES

Angonin-Willaime M.-C., Soucail G., Vanderriest C., 1994,

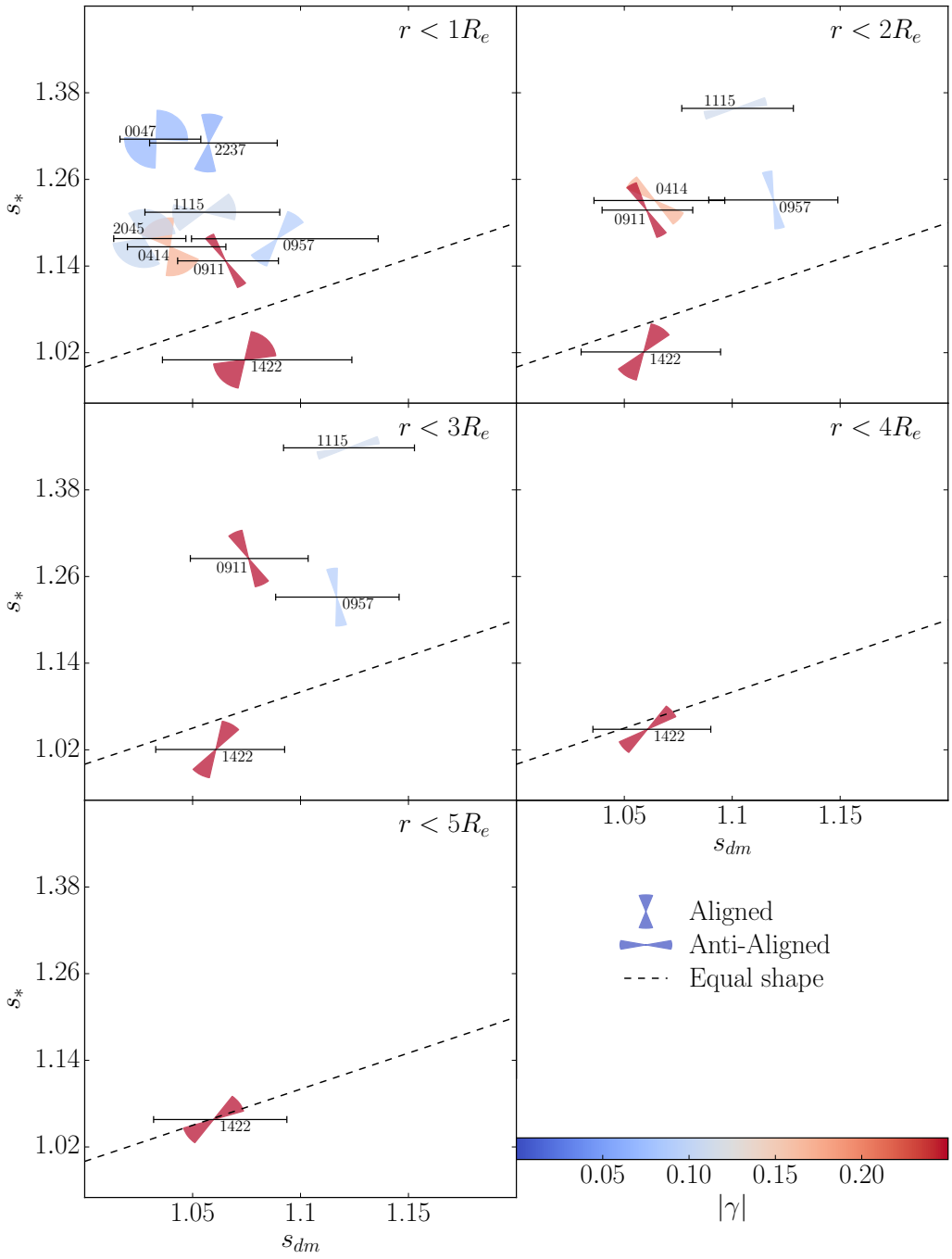

Figure 2. Similar to Figure 1. In each of the subfigures however we only consider pixels within 1, 2, 3, 4, or 5 R_e. If a lens does not extend to these limiting radii, it is dropped from the analysis in this and subsequent subfigures.

A&A, 291, 411

Auger M. W., Fassnacht C. D., Abrahamse A. L., Lubin L. M., Squires G. K., 2007, AJ, 134, 668

Auger M. W., Treu T., Bolton A. S., Gavazzi R., Koopmans L. V. E., Marshall P. J., Moustakas L. A., Burles S., 2010, ApJ, 724, 511

Barkana R., 1997, ApJ, 489, 21

Blandford R., Narayan R., 1986, ApJ, 310, 568

Brainerd T. G., Wright C. O., 2000, ArXiv Astrophysics e-prints

Chartas G., Chuss D., Forman W., Jones C., Shapiro I., 1998, ApJ, 504, 661

Coles J., 2008, ApJ, 679, 17

Coles J. P., Read J. I., Saha P., 2014, ArXiv e-prints

Curran S. J., Whiting M. T., Tanna A., Bignell C., Webb J. K., 2011, MNRAS, 413, L86

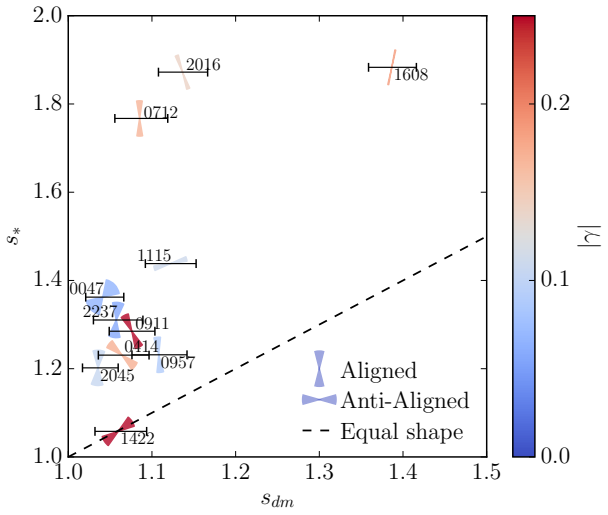

Figure 1. The reconstructed lenses are displayed according to the reconstructed total shapes of the dark matter halo s_{dm} and the stellar component s_*. The wedges display the alignment of the semi-major axes of the components. In case of alignment of the semi-major axes (Aligned), the wedges are vertical. In case of alignment of the semi-major with the semi-minor axes (Anti-Aligned), the wedges are horizontal. The opening angle displays the error in the shape estimate of the dark matter halo. The lenses are additional color-coded in terms of the required external shear in modelling the lens.

Dai X., Kochanek C. S., 2005, ApJ, 625, 633
Debattista V. P., Moore B., Quinn T., Kazantzidis S., Maas R., Mayer L., Read J., Stadel J., 2008, ApJ, 681, 1076
Debattista V. P., Roškar R., Valluri M., Quinn T., Moore B., Wadsley J., 2013, MNRAS, 434, 2971
Dubinski J., 1994, ApJ, 431, 617
Dubinski J., Carlberg R. G., 1991, ApJ, 378, 496
Fassnacht C. D. et al., 1999, AJ, 117, 658
Fassnacht C. D., Cohen J. G., 1998, AJ, 115, 377
Fassnacht C. D., Gal R. R., Lubin L. M., McKean J. P., Squires G. K., Readhead A. C. S., 2006, ApJ, 642, 30
Fassnacht C. D., Xanthopoulos E., Koopmans L. V. E., Rusin D., 2002, ApJ, 581, 823
Ferreras I., Mavromatos N. E., Sakellariadou M., Yusaf M. F., 2012, Phys. Rev. D, 86, 083507
Ferreras I., Saha P., Burles S., 2008, MNRAS, 383, 857
Ferreras I., Saha P., Williams L. L. R., 2005, ApJ, 623, L5
Garrett M. A., Walsh D., Carswell R. F., 1992, MNRAS, 254, 27P
Grant C. E., Bautz M. W., Chartas G., Garmire G. P., 2004, ApJ, 610, 686
Helmi A., 2004, ApJ, 610, L97
Hjorth J. et al., 2002, ApJ, 572, L11
Hoekstra H., Yee H. K. C., Gladders M. D., 2004, ApJ, 606, 67
Ibata R., Lewis G. F., Irwin M., Totten E., Quinn T., 2001, ApJ, 551, 294
Impey C. D., Foltz C. B., Petry C. E., Browne I. W. A., Patnaik A. R., 1996, ApJ, 462, L53
Jing Y. P., Suto Y., 2002, ApJ, 574, 538
Katz N., Gunn J. E., 1991, ApJ, 377, 365
Kazantzidis S., Kravtsov A. V., Zentner A. R., Allgood B., Nagai D., Moore B., 2004, ApJ, 611, L73
Keeton C. R. et al., 2000, ApJ, 542, 74
Keeton C. R., Kochanek C. S., Falco E. E., 1998, ApJ, 509, 561
Kneib J.-P., Cohen J. G., Hjorth J., 2000, ApJ, 544, L35
Kochanek C. S. et al., 2000, ApJ, 543, 131
Koopmans L. V. E., Treu T., Bolton A. S., Burles S., Moustakas L. A., 2006, ApJ, 649, 599
Lawrence C. R., Schneider D. P., Schmidt M., Bennett C. L., Hewitt J. N., Burke B. F., Turner E. L., Gunn J. E., 1984, Science, 223, 46
Leier D., 2011, PhD thesis, Astronomisches Rechen-Institut, Zentrum für Astronomie der Universität Heidelberg
Leier D., Ferreras I., Saha P., 2012, MNRAS, 424, 104
Leier D., Ferreras I., Saha P., Falco E. E., 2011, ApJ, 740, 97
Lubini M., Coles J., 2012, MNRAS, 425, 3077
Lux H., Read J. I., Lake G., Johnston K. V., 2012, MNRAS, 424, L16
Macciò A. V., Dutton A. A., van den Bosch F. C., Moore B., Potter D., Stadel J., 2007, MNRAS, 378, 55
Mandelbaum R., Hirata C. M., Broderick T., Seljak U., Brinkmann J., 2006, MNRAS, 370, 1008
McKean J. P. et al., 2007, MNRAS, 378, 109
Momcheva I., Williams K., Keeton C., Zabludoff A., 2006, ApJ, 641, 169
Morgan N. D., Chartas G., Malm M., Bautz M. W., Burud I., Hjorth J., Jones S. E., Schechter P. L., 2001, ApJ, 555, 1
Mortlock D. J., Turner E. L., 2001, MNRAS, 327, 552
Natarajan P., Refregier A., 2000, ApJ, 538, L113
Navarro J. F., Frenk C. S., White S. D. M., 1996, ApJ, 462, 563
Parker L. C., Hoekstra H., Hudson M. J., van Waerbeke L., Mellier Y., 2007, ApJ, 669, 21
Patnaik A. R., Narasimha D., 2001, MNRAS, 326, 1403
Raychaudhury S., Saha P., Williams L. L. R., 2003, AJ, 126, 29
Read J. I., 2014, Journal of Physics G Nuclear Physics, 41, 063101
Read J. I., Moore B., 2005, MNRAS, 361, 971
Saha P., Williams L. L. R., 2004, AJ, 127, 2604
Schechter P. L., Moore C. B., 1993, AJ, 105, 1
Schneider D. P., Gunn J. E., Turner E. L., Lawrence C. R., Hewitt J. N., Schmidt M., Burke B. F., 1986, AJ, 91, 991
Schneider P., Ehlers J., Falco E. E., 1992, Gravitational Lenses
Shalyapin V. N., Goicoechea L. J., Gil-Merino R., 2012, A&A, 540, A132
Sluse D., Chantry V., Magain P., Courbin F., Meylan G., 2012, A&A, 538, A99
Surpi G., Blandford R. D., 2003, ApJ, 584, 100
Toft S., Soucail G., Hjorth J., 2003, MNRAS, 344, 337
Tonry J. L., Kochanek C. S., 1999, AJ, 117, 2034
Treu T., Gavazzi R., Gorecki A., Marshall P. J., Koopmans L. V. E., Bolton A. S., Moustakas L. A., Burles S., 2009, ApJ, 690, 670
Treu T., Koopmans L. V., Bolton A. S., Burles S., Moustakas L. A., 2006, ApJ, 640, 662
Tsvetkova V. S. et al., 2010, MNRAS, 406, 2764

van Uitert E., Hoekstra H., Schrabback T., Gilbank D. G., Gladders M. D., Yee H. K. C., 2012, A&A, 545, A71
Warren M. S., Quinn P. J., Salmon J. K., Zurek W. H., 1992, ApJ, 399, 405
Warren S. J., Hewett P. C., Lewis G. F., Moller P., Iovino A., Shaver P. A., 1996, MNRAS, 278, 139
Wong K. C., Keeton C. R., Williams K. A., Momcheva I. G., Zabludoff A. I., 2011, ApJ, 726, 84
Yee H. K. C., 1988, AJ, 95, 1331
Yoo J., Kochanek C. S., Falco E. E., McLeod B. A., 2005, ApJ, 626, 51

APPENDIX A: RECONSTRUCTED LENSES

In this appendix, we show the results of our lens modelling for each individual lens (Figures A1, A2, and A3). The panels show, from left to right: the arrival time surface; the surface mass density of the dark matter; and the surface mass density of the stars. The solid lines mark the eigenvalues and eigenvectors of the 2D moment of inertia tensor in each case; the dotted lines the 68% confidence interval of these for the dark matter map. Figure 1 is constructed from the ratio of largest to smallest eigenvalue in each case (to measure the shape parameter s), and the angle between the dark matter and stellar major axes. Note that the angular scale is always the same for the dark matter and stellar maps, but varies between the different lenses as marked on the Figure axes.

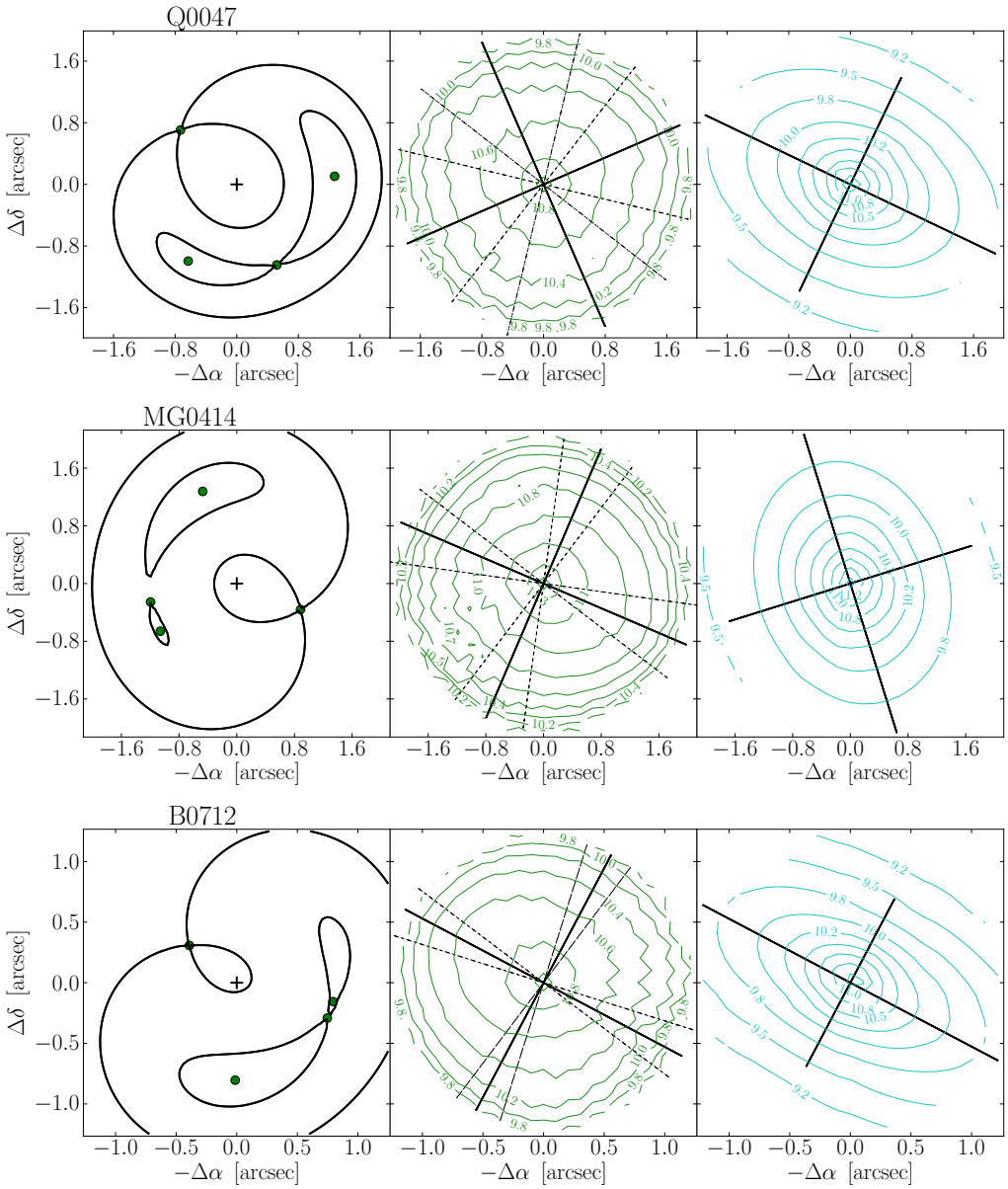

Figure A1. The results of our lens modelling for each individual lens. The panels show, from left to right: the arrival time surface (the images are marked by the green circles); the surface mass density of the dark matter; and the surface mass density of the stars. The solid lines mark the eigenvalues and eigenvectors of the 2D moment of inertia tensor in each case; the dotted lines the 68% confidence interval of these for the dark matter map.

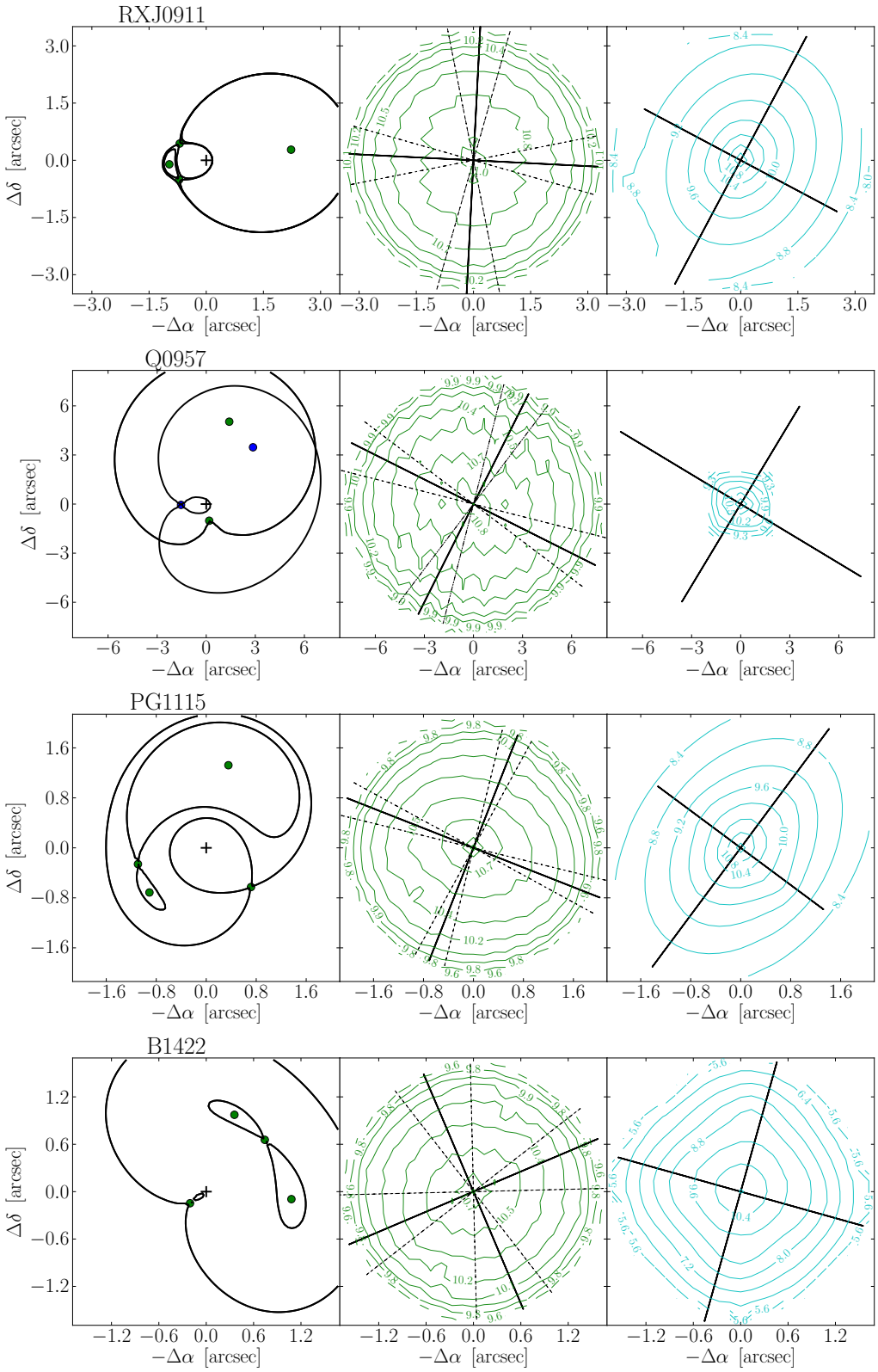

Figure A2. The results of our lens modelling for each individual lens. Lines and symbols are as in Figure **??**.

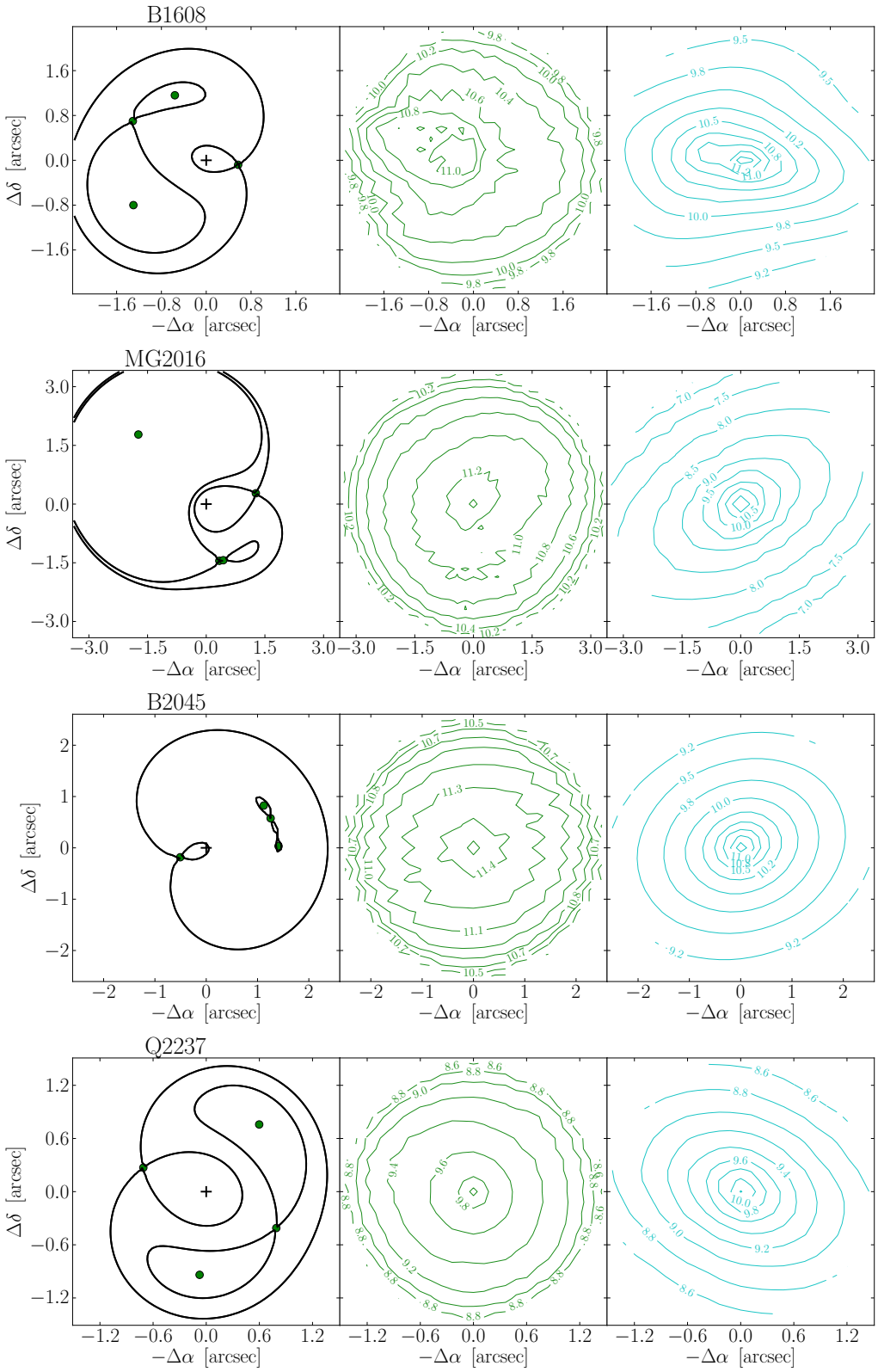

Figure A3. The results of our lens modelling for each individual lens. Lines and symbols are as in Figure **??**.